

Reducing Heat Duty of MEA Regeneration Using a Sulfonic Acid-Functionalized Mesoporous MCM-41 Catalyst

Qiang Sun, Tianhao Li, Yu Mao, Hongxia Gao,* Teerawat Sema, Shengyu Wang, Libin Liu, and Zhiwu Liang*



Cite This: *Ind. Eng. Chem. Res.* 2021, 60, 18304–18315



Read Online

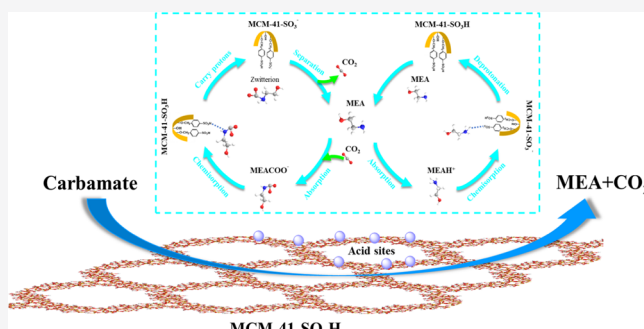
ACCESS |

Metrics & More

Article Recommendations

Supporting Information

ABSTRACT: Amine-based CO₂ capture is a promising method to limit global CO₂ emissions. However, large thermal energy consumption for CO₂ desorption during amine regeneration has limited large-scale worldwide applications. Here, we show that an efficient MCM-41-SO₃H-0.6 catalyst presented a superior catalytic performance, decreasing the relative heat duty by one-third and enhancing the instantaneous desorption rate by up to 195% in comparison with the monoethanolamine (MEA) regeneration without catalysts. The excellent catalytic activity is related to the combination of the properties of mesopore surface area × total acid sites, and a possible catalytic mechanism is proposed for the MCM-41-SO₃H catalysts. Furthermore, the experimental results in the MEA solution regeneration process were consistent with density functional theory calculations in revealing the catalytic desorption mechanism. This work demonstrated that MCM-41 functionalized with sulfonic acid group catalysts could play an essential role in the post-combustion CO₂ capture technology using aqueous MEA for industrial applications.



1. INTRODUCTION

The combustion of fossil fuels to meet the rapidly growing energy demand due to the development of the economy and society releases CO₂ and leads to environmental pollution.¹ Regarding global warming, carbon capture and storage (CCS) is considered a potential way to reduce the emission of CO₂ and limit warming to less than 2 °C.^{2,3} Typically, the technology for CO₂ capture can be divided into three main processes, including pre-combustion, post-combustion, and oxy-fuel.^{4,5} Among these technologies, post-combustion CO₂ capture using aqueous amine solutions is the most applicable and mature approach to mitigate CO₂ emission. It can be retrofitted into current power plants and can treat large flue gas steams.^{6,7}

As is well known, monoethanolamine (MEA) has been widely used in the thermal amine scrubbing technology because of its fast absorption kinetics, high cyclic capacity, and cheap price.⁸ However, this technology has some limitations, including amine degradation and equipment corrosion.⁹ However, the major drawback of MEA-based chemical absorption is the high energy requirement during amine regeneration for CO₂ desorption, which accounts for more than two-thirds of the entire operating cost for CO₂ capture and limits further commercial applications.¹⁰ Therefore, the reduction of the heat duty for CO₂ desorption is a big challenge to deal with in the field of CCS technology.

According to previously reported work, the energy consumption of MEA-based CO₂ capture for CO₂ desorption includes energy for sensible, vaporization, and desorption heat.^{11,12} First, the sensible heat is related to the energy required for increasing the temperature of CO₂-rich amine. Second, the vaporization heat is ascribed to vaporizing the MEA solvent for CO₂ desorption. Third, the desorption heat is used to break the chemical bond between CO₂ and MEA, which account for approximately 50% of the total energy consumption of 5 M CO₂-rich MEA regeneration.¹³ To reduce the energy consumption for amine regeneration, much effort has been put into solving this problem, such as screening for a novel amine,^{14–16} using blended amine,¹⁷ designing for better mass and heat transfer,¹⁸ optimizing the process configuration,^{19,20} and developing biphasic solvents.^{21–23}

In addition, the process of MEA regeneration is a strongly endothermic reaction, and the rate-limiting step mainly includes two parts: carbamate breakdown and MEAH⁺ deprotonation.²⁴ It is generally accepted that the acceleration of proton transfer in CO₂ desorption systems can assist the

Received: September 11, 2021

Revised: December 1, 2021

Accepted: December 1, 2021

Published: December 13, 2021



MEA regeneration process.²⁵ The reason for this is that the deprotonation of MEAH⁺ is difficult due to the pH of MEA being higher than neutral water, which leads to a lack of free protons, and the reaction of carbamate decomposition is unable to occur at low temperatures.²⁶ Recently, it has been reported that the heat duty of MEA regeneration can be reduced by acid catalysis, which improves proton transfer, decreases the activation energy for carbamate decomposition, and reduces the required temperature for CO₂ desorption to less than 100 °C.²⁷

Concerning homogeneous catalysis, mineral acids such as oxalic acid, suberic acid, and phthalic acid or Lewis acids such as CuCl₂ and NiCl₂ are useful for CO₂ desorption.^{28,29} Even though these acids can reduce the overall energy requirement and advance the process of MEA regeneration, the drawback of this method is that the activated component is difficult to separate and thus unavailable for reuse. Another drawback of mineral acids is reactor corrosion, which might lead to environmental problems and limit industrial applications.

To avoid environmental hazards and solve the separation problems, heterogeneous catalytic processes for CO₂ desorption using solid acid catalysts have been widely investigated in MEA-based post-combustion CO₂ capture.³⁰ Different types of solid acid catalysts have been added to CO₂-rich amine to enhance the desorption rate, such as metal-organic frameworks,³¹ carbonic anhydrase,³² transition-metal oxides,^{33,34} sulfated metal oxides,³⁵ and hydroxy metal oxides.³⁶ Among these solid acid catalysts, the zeolite molecular sieves focus on abundant research because of their high surface area, hydrothermal stability, and controllable acid strength.^{37,38} However, the zeolite molecular sieves possess low intrinsic acidity, limiting their catalytic efficiency in MEA regeneration, because the catalytic CO₂ desorption is influenced by the quantities of acid sites in catalysts.³³

Therefore, various methods have been proposed to improve the acidity of zeolite molecular sieves, including alkaline desilication, loading sulfated metal oxides, modification with metals, and so forth. Bhatti *et al.*³⁹ improved the acidity and mesoporosity of a series of HZSM-5 catalysts through desilication methods using alkaline media to accelerate the proton-transfer rate and increase the quantity of CO₂ desorbed by up to 60%. Gao *et al.*⁴⁰ synthesized SO₄²⁻/ZrO₂/SBA-15 catalysts and exhibited superior catalytic activity in amine regeneration, decreasing the energy requirement by 20–26.5% compared to the blank run. Xing *et al.*²⁵ reported the SO₄²⁻/ZrO₂-HZSM-5 catalyst and improved the CO₂ cyclic capacity and desorption rate by 40 and 37%. Zhang *et al.*²⁶ designed catalysts of MCM-41 modified with Fe, Al, and Mo metals and significantly improved the CO₂ desorption rate with the reduction of the relative heat duty by 32.5% at 98 °C.

In this work, the well-known ordered mesoporous zeolites, namely, MCM-41 catalysts, were functionalized with sulfonic acid groups by post-synthesis methods compared to sulfuric acid MCM-41 silica catalysts. The synthesized catalysts were characterized by X-ray diffraction (XRD), N₂ adsorption-desorption, Fourier transform infrared (FT-IR) spectroscopy, thermogravimetry (TG), scanning electron microscopy (SEM), and acid-base titration. The catalytic performance of the novel MCM-41-SO₃H catalysts for CO₂ desorption in the rich MEA solvent was then systematically studied in terms of the desorption rate, the amount of desorbed CO₂, and the relative heat duty. A plausible mechanism of MCM-41-SO₃H catalysts is proposed to explain the catalytic process of

carbamate breakdown and CO₂ release. Moreover, the effect of different physicochemical properties and the stability of catalysts were also studied.

2. EXPERIMENTAL SECTION

2.1. Materials. MEA (99%) and benzyl alcohol (\geq 99%) were obtained from Aladdin Industrial Corporation, China. MCM-41 white powder was obtained from NanKai University Catalyst Co. Ltd., China. Chlorosulfonic acid (>97%, GC) was purchased from TCI Shanghai Co. Ltd., China. Toluene (\geq 99.5%) and trichloromethane (\geq 99%) were supplied by Sinopharm Chemical Reagent Co. Ltd., China. CO₂ (99.9%) and N₂ (99.99%) were purchased from Changsha Rizhen Gas Co. Ltd., China.

2.2. Catalyst Preparation. **2.2.1. Preparation of the SO₄²⁻/MCM-41 Catalyst.** The SO₄²⁻/MCM-41 catalyst was synthesized using the impregnation method. Briefly, 10 g of powder MCM-41 was added into 150 mL of 1 M H₂SO₄ solution and stirred for 3 h at room temperature. After that, the solvent was evaporated at 110 °C. Finally, the white solid was calcined in air at 550 °C for 3 h to prepare the SO₄²⁻/MCM-41 catalyst.

2.2.2. Preparation of the MCM-41-SO₃H Catalyst. The one-pot synthetic procedure of MCM-41 functionalized with sulfonic acid groups was based on the previously reported method with a slight modification.⁴¹ The detailed information of catalyst preparation in this work is as follows: first, 10 g of powder of MCM-41 was added into the mixed solvent of 200 mL of toluene and 50 mL of benzyl alcohol, and then, the mixture was stirred and heated with reflux for 12 h at 120 °C. Second, the suspension was separated by centrifugation and dried at 60 °C for 12 h. Third, the obtained powder solid was introduced into 200 mL of trichloromethane solution, and then, the proper amount of chlorosulfonic acid was added dropwise into the suspension while stirring at room temperature. Fourth, the reactants were stirred and refluxed at 70 °C for 2 h and then centrifuged and washed with dry trichloromethane three times. Finally, the MCM-41-SO₃H catalysts were obtained by drying the solids under vacuum at 60 °C for 12 h. The catalysts synthesized with varied contents of chlorosulfonic acid were labeled as MCM-41-SO₃H-*x*, where *x* represents the ratio of the volume of chlorosulfonic acid to the mass of the MCM-41 molecular sieve (mL/g).

2.3. Material Characterization and Computational Methods. XRD was performed with a Rigaku Ultimate IV and XRD-6100 diffractometer using Cu K α radiation in the range of $2\theta = 0.5\text{--}10^\circ$ with a speed at 1°/min and $2\theta = 10\text{--}80^\circ$ with a speed at 8°/min. N₂ adsorption-desorption isotherms were determined using AUTOSORB IQ equipment at 77 K. Before each adsorption, the samples were degassed at 60 °C for 6 h under vacuum. The surface area was calculated by the Brunauer–Emmett–Teller method, and the pore size distribution was measured using the Barrett–Joyner–Halenda model. The FT-IR spectra were obtained on an IR Affinity-1 spectrophotometer using the KBr pellet technique with the region from 4000 to 400 cm⁻¹. Thermo-gravimetric analysis was performed by using a NETZSCH STA 2500 Regulus, aiming to analyze the weight change of the sample during heating. The sample was heated to 750 °C at a ramp of 5 °C/min under N₂ at 50 mL/min. SEM images were detected with a COXEM EM-30 instrument. The sulfur contents of the recovered catalyst were measured by inductively coupled plasma optical emission spectroscopy, which was performed

using Agilent 720ES equipment. The total acid sites (TASs) of the catalysts were measured by the acid–base titration method as reported.⁴¹ Briefly, 0.05 g of the solid was mixed with 15 mL of 2 M NaCl and kept under constant stirring, and then, the acid sites were determined by 0.01 M NaOH titration.

All calculations in the paper were spin-polarized and carried out with the Perdew–Burke–Ernzerhof⁴² functional using the Vienna *ab initio* simulation package.^{43,44} The D3 correction method⁴⁵ was employed to include van der Waals interactions. The project-augmented wave method was used to represent the core–valence interaction.^{46,47} For the calculations of total energy, a cutoff energy of 450 eV was set for plane-wave basis sets to expand the valence electronic states, and the converging criteria of the force on each relaxed atom below 0.05 eV/Å were used for structural optimizations. The lattice parameter for the MCM-41 unit cell is $a = 40.60$, $b = 40.60$, $c = 12.20$ Å, and the chemical formula of the unit cell is $\text{Si}_{142}\text{O}_{335}\text{H}_{102}$ (579 atoms in total). All atoms are fully relaxed during optimization, and the Brillouin zone is restricted to $1 \times 1 \times 1$ (γ -point).

2.4. Experimental Apparatus and Procedure for CO₂ Desorption.

The experimental apparatus used for the CO₂ desorption is presented in Figure 1, mainly including a reactor,

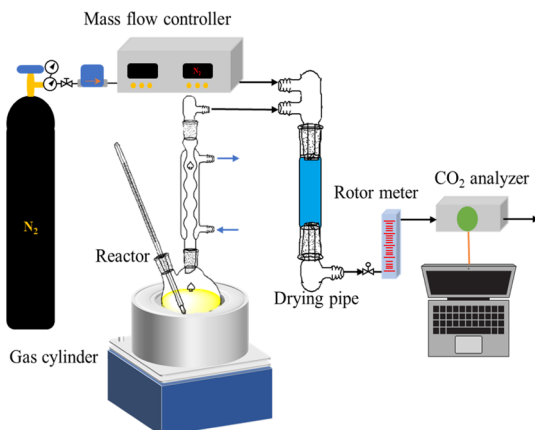


Figure 1. Schematic of the apparatus for the CO₂ desorption process.

a mass flow controller (model D07, Beijing Sevenstar), a heating mantle, and a CO₂ analyzer (model GS10, Ennix, Germany, accuracy of 1%). A 1000 mL round-bottomed flask with a heating mantle was used as a batch reactor. A thermocouple was put into the flask to measure the temperature of the MEA solution, and a condenser was connected to the flask in order to minimize MEA solution loss. A magnetic stirrer was used to ensure sufficient interfacial contact between the solid catalysts and the amine liquid at a stirring speed of 1200 rpm. The CO₂ desorbed from the MEA solvent was dried by silica gel and mixed with nitrogen carrier gas (1 L/min), and then, the CO₂ concentration was determined using an infrared CO₂ analyzer every 10 s. Moreover, the energy consumption for MEA regeneration was recorded using a power meter (Zhejiang Tepsung Electric Co. Ltd., an accuracy of 0.001 kW·h) monitoring the energy input to the heater, and the heat mantle and the heating preservation cotton were made a body to prevent energy loss. The residual CO₂ in the apparatus tubing was purged with N₂ before and after every experiment.

For a typical desorption test, 500 mL of 5 M CO₂-rich MEA with an initial CO₂ loading (0.52 mol CO₂/mol amine) and

6.25 g of the catalyst to give a mass ratio of catalyst to amine solution of 1.25 wt % were introduced into the reactor. Subsequently, the solution was heated to a temperature of 90.5 ± 0.1 °C, and the desorption experiment was run for 1 h. In this work, the CO₂-rich amine solvent was taken from only one batch so as to reduce the error. The CO₂ loading was obtained using the Chittick apparatus,⁴⁸ for which the average absolute relative deviation was lower than 5%. For each sample, the CO₂ loading was titrated twice to guarantee the accuracy of data. At the same time, the quantities of CO₂ desorbed obtained by both the gas phase and liquid phase were compared to verify the conservation of mass.

2.5. Data Calculation Method. The CO₂ desorption rate [mol/(s L)] can be calculated on the basis of the CO₂ concentration collected by the CO₂ analyzer using eq 1

$$r = \frac{1}{22.4 \times V} \left(v_{\text{N}_2}^{\text{in}} \times \frac{X_{\text{CO}_2}^{\text{out}}}{1 - X_{\text{CO}_2}^{\text{out}}} \right) \quad (1)$$

where r is the CO₂ desorption rate [mol/(s L)], V is the volume of the desorbed MEA solution (L), $v_{\text{N}_2}^{\text{in}}$ is the flow rate of N₂ (L/min), and $X_{\text{CO}_2}^{\text{out}}$ is the volumetric fraction of CO₂ in the outlet gas.

The amount of CO₂ desorbed from CO₂-rich MEA solution can be calculated using eq 2

$$n_{\text{CO}_2}(t) = V \int_0^t r \, d\,t \quad (2)$$

where n_{CO_2} is (mmol) the amount of CO₂ desorbed at time t (s).

The heat duty for the CO₂ desorption can be calculated using eq 3, and the energy consumption was recorded using a power meter

$$\text{HD} = \frac{E(t)}{n_{\text{CO}_2}(t)} \quad (3)$$

where HD is the heat duty for MEA regeneration (kJ/mol) and $E(t)$ is the amount of energy consumed by the heating mantle to heat the MEA solution at time t (kJ).

The HD values calculated in this work may be higher than the actual heat duty because of the simplified desorption apparatus. Thus, the relative heat duty is used to give a better comparison of energy consumption for the MEA regeneration process, as shown in eq 4,

$$\text{RH} = \frac{\text{HD}_i}{\text{HD}_{\text{baseline}}} \times 100\% \quad (4)$$

where RH is the relative heat duty for the CO₂ desorption (%), HD_i is the HD of the CO₂-rich MEA solution with different catalysts in the first 1200 s (kJ/mol), and HD_{baseline} is the HD of the CO₂-rich MEA solution without the catalyst in the first 1200 s (kJ/mol).

3. RESULTS AND DISCUSSION

3.1. Characterization of Catalysts. 3.1.1. XRD and SEM.

The X-ray diffractograms of MCM-41 and MCM-41-SO₃H are shown in Figures 2a and S1. It can be observed that all the diffractograms possessed the characteristic peak of MCM-41, which indicates that the crystallographic ordering of the mesoporous structure of MCM-41 remained after being functionalized with sulfonic acid groups. It can be seen that

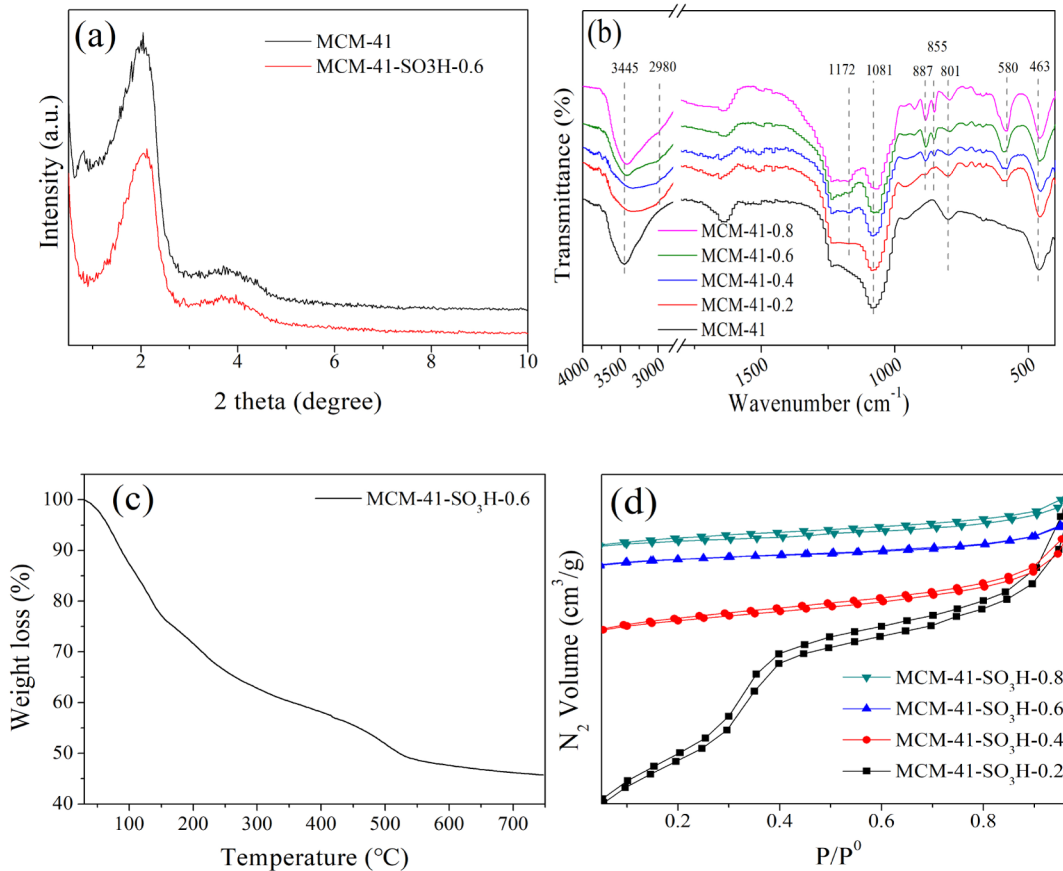


Figure 2. (a) XRD curves. (b) FT-IR spectra. (c) TG curve of the MCM-41-SO₃H-0.6 catalyst. (d) N₂ adsorption–desorption isotherms.

the peak intensity of MCM-41-SO₃H was weaker than that of MCM-41, which implies that the pore structure of MCM-41-SO₃H may be reduced due to the introduction of organic groups.

The morphological analyses of MCM-41 and MCM-41-SO₃H-0.6 are compared in Figure S2. The SEM images revealed that MCM-41 presented a squamous structure, while the MCM-41-SO₃H-0.6 catalyst has a uniform size with a low agglomeration trend. These results indicate that the organic groups may block some mesoporous channels of MCM-41, as also demonstrated by N₂ adsorption–desorption isotherms.

3.1.2. FT-IR Spectroscopy and TG Analysis. Figure 2b displays the FT-IR spectrum of MCM-41 and MCM-41-SO₃H. The wide band at about 3445 cm⁻¹ is related to the asymmetric vibrations of –OH groups of the absorbed water and surface silanol.⁴⁹ Three peaks at about 1081, 801, and 463 cm⁻¹ relate to the asymmetric, symmetric, and bending vibrations of M–O–M bonds (M = Al, Si), respectively.²⁶ Moreover, the peaks attributed to the sulfonic acid group and benzene ring are visible in the spectrum of MCM-41-SO₃H. The peaks located at about 2980 cm⁻¹ correspond to the stretching vibrations of C–H bonds of benzyl, while the presence of bands at about 887 and 855 cm⁻¹ corresponds to the bending vibrations of benzene.⁴¹ The bands at 1172 cm⁻¹ are ascribed to the symmetrical stretch of the SO₂ bond, and the bands at 580 cm⁻¹ are attributed to the stretching vibrations of S–O bonds. To sum up, the existence of a benzene ring was confirmed in the catalysts, and the sulfonic acid groups were introduced into the surface of the MCM-41 molecular sieve successfully.

The TG curve of the synthesized MCM-41-SO₃H-0.6 catalyst is displayed in Figure 2c. The weight loss in 30–150 °C regions is attributed to removing the residual organic solvent during the catalyst synthesis and the physically absorbed water. The weight loss in the region of 150–550 °C is ascribed to the decomposition of the organic groups. The results demonstrate that the sulfonic acid groups had been successfully anchored to the surface of MCM-41, which is consistent with the FT-IR results. However, these processes are unlikely to occur at the temperature used in our catalytic tests, which can be confirmed by the superior stability during the CO₂ desorption experiments.

3.1.3. Textural Properties. The N₂ adsorption–desorption isotherms for MCM-41-SO₃H catalysts are compared in Figure 2d, and the results are listed in Table 1. All the isotherms exhibit isotherms of type IV, which are related to the existence of the mesoporous structure. It can be observed that the

Table 1. Textural Properties and Acidity of Different Catalysts

catalysts	mesopore surface area (m ² /g)	average pore diameter (nm)	pore volume (cm ³ /g)	total acid sites (mmol/g)
MCM-41	1058.6 ²⁶	3.04 ²⁶	1.00 ²⁶	0.19
SO ₄ ²⁻ /MCM-41	451 ⁵⁰	3.7 ⁵⁰	0.7 ⁵⁰	0.23
MCM-41-SO ₃ H-0.2	117.80	3.06	0.14	0.41
MCM-41-SO ₃ H-0.4	23.36	3.37	0.045	2.35
MCM-41-SO ₃ H-0.6	13.87	3.42	0.023	4.76
MCM-41-SO ₃ H-0.8	11.12	3.39	0.025	5.27

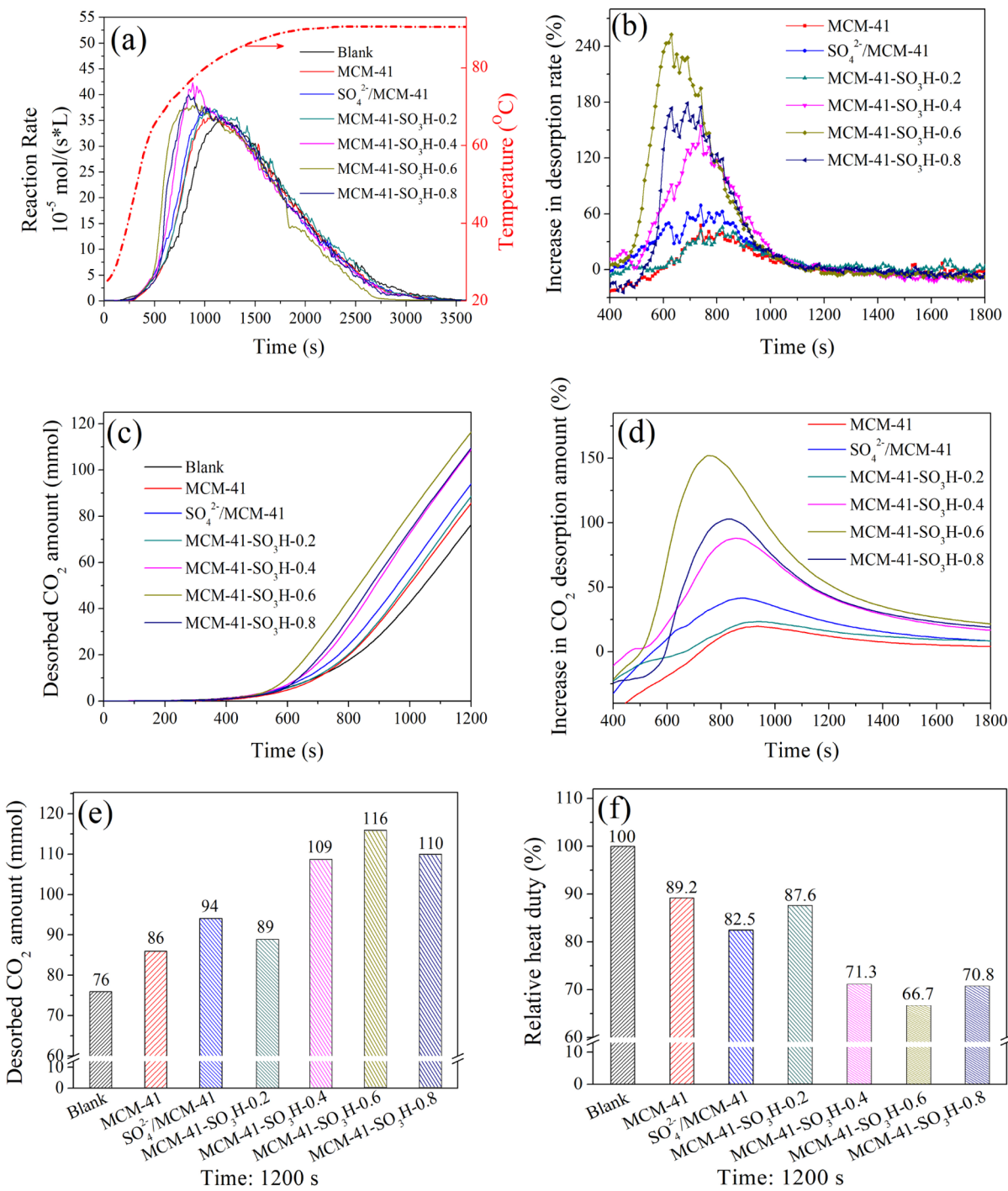


Figure 3. CO₂ desorption performance with and without catalysts at 90 °C. (a) CO₂ desorption rate curves. (b) Percentage increases in the CO₂ desorption rate due to the use of catalysts. (c) Desorbed CO₂ amount curves. (d) Percentage increases in the CO₂ desorption amount due to the use of catalysts. (e) Total amount of CO₂ desorbed at 1200 s. (f) Relative heat duty.

surface area of MCM-41-SO₃H was sharply reduced with increasing concentration of the sulfonic acid groups. Moreover, when the ratio of the volume of chlorosulfonic acid to the mass of MCM-41 was more than 0.2 mL/g, a significant reduction of surface area from 117.80 to 23.36 m²/g was observed between MCM-41-SO₃H-0.2 and MCM-41-SO₃H-0.4 catalysts. The possible reason for this is that the benzyl sulfonic acid chains protruding from the walls into the channels were closely packed, which led to aggregation and partial structural collapse. In addition, the average pore diameter of MCM-41-SO₃H

catalysts was larger than that in MCM-41, and it is confirmed that the average pore diameter was at maximum with the MCM-41-SO₃H-0.6 catalyst at 3.42 nm. This may be due to the acid etching caused by the chlorosulfonic acid used in the synthesis. However, the crystalline structure of MCM-41 was well maintained in MCM-41-SO₃H, which is confirmed by XRD results.

3.1.4. Acidity Properties. The amount of TAs for the samples as obtained by titration is listed in Table 1. It is worth noting that the acid sites increased after MCM-41 was

functionalized with sulfonic acid groups which could donate protons and can be inferred as Brønsted acid sites. As displayed in the results, the TASs correlated with the amount of chlorosulfonic acid introduced into MCM-41. It is noted that the quantities of TASs of MCM-41-SO₃H were enhanced compared with MCM-41, which suggests that the sulfonic acid groups were immobilized to the surface of the molecular sieve successfully and led to varied acidity. Also, the catalysts functionalized with sulfonic acid groups possess large amounts of acid sites than the parent MCM-41 and untreated SO₄²⁻/MCM-41 catalysts. Moreover, for all the samples, the higher the ratio of the volume of chlorosulfonic acid to the mass of MCM-41, the greater the quantity of acid sites that resulted. MCM-41-SO₃H-0.8 had the most acid sites at 5.27 mmol/g, while the amount of acid sites of MCM-41 and SO₄²⁻/MCM-41 was only 0.19 and 0.23 mmol/g, respectively. Notably, the acid sites were provided from the sulfonic acid groups and necessary for the catalytic performance.

3.2. CO₂ Desorption Performance. The CO₂ desorption rates of CO₂-rich MEA solution with and without the catalyst are displayed in Figure 3. It can be seen that all the catalysts increased the desorption rate and the amount of CO₂ desorbed. The CO₂ desorption rate profiles reached a maximum peak at about 1200 s and then decreased for all systems. Thus, the CO₂ desorption over the first 1200 s was selected to evaluate the catalytic performance, and the CO₂-rich MEA without the catalyst provided a baseline with which to compare the effectiveness of the catalysts.

As shown in Figure 3a, the peak CO₂ desorption rate of CO₂-rich MEA solution without the catalyst was 3.487×10^{-4} mol/(s L) at 1150 s. The maximum desorption rate of the SO₄²⁻/MCM-41 catalyst was 3.715×10^{-4} mol/(s L) at 1030 s, showing a slight improvement compared with the blank run. MCM-41-SO₃H-0.2 slightly improved the CO₂ desorption rate and achieved its maximum of 3.716×10^{-4} mol/(s L) at 1100 s, and the value of the CO₂ desorption rate peak was 4.231×10^{-4} mol/(s L) at 880 s for the MCM-41-SO₃H-0.4 catalyst. Moreover, the peak desorption rates of the CO₂-rich solution with MCM-41-SO₃H-0.6 and MCM-41-SO₃H-0.8 catalysts were 3.827×10^{-4} and 3.999×10^{-4} mol/(s L) at 910 and 840 s, respectively.

It can be concluded that all the catalysts reached the maximum desorption rate earlier than the blank run, and the value of the peak CO₂ desorption rate was higher than that for the MEA solution without catalysts. The percentage increase in the CO₂ desorption rate attributed to the MCM-41-SO₃H catalysts as a function of time is illustrated in Figure 3b. At 740 s, the percentage improvement of desorption rate of MCM-41-SO₃H-0.2 and MCM-41-SO₃H-0.4 was 41 and 154% over that of the baseline MEA solution without the catalyst, respectively, and the enhancement of that for MCM-41-SO₃H-0.8 was 174% higher than that for the blank run. However, the MCM-41-SO₃H-0.6 catalyst possessed the largest increase as high as 194% at the same point. Therefore, the MCM-41-SO₃H-0.6 catalyst best accelerated the proton transfer and best enhanced the CO₂ desorption rate.

In addition to the CO₂ desorption rate, Figure 3c presents the influence of the catalysts on CO₂ desorption curves, and the improvement in CO₂ desorption amount is exhibited in Figure 3d with the increase in the amount of CO₂ desorbed at the same time interval. Also, the amounts of CO₂ desorbed in the first 1200 s are compared in Figure 3e. Only 76 mmol CO₂ was desorbed from CO₂-rich MEA solution without the

catalyst, and 86 mmol CO₂ was released when MCM-41 was used. MCM-41-SO₃H-0.2 slightly enhanced the CO₂ desorbed amount to 89 mmol, and the quantities of CO₂ desorption attributed to the use of MCM-41-SO₃H-0.4 and MCM-41-SO₃H-0.8 were 109 and 110 mmol, respectively. The best performance was exhibited by MCM-41-SO₃H-0.6, which led to a CO₂ desorption amount of 116 mmol, 53% higher than that for CO₂-rich MEA solution without the catalyst. Therefore, all the MCM-41-SO₃H catalysts are capable of desorbing greater amounts of CO₂ compared to the blank run, thus reducing the heat duty of MEA solution regeneration because the heat duty is related to the quantity of CO₂ desorbed per unit of energy consumption. Also, it would be a necessary work to investigate the solid catalyst introduced into an operating CO₂ catalytic desorber and optimize the catalytic desorption conditions for industrial applications. The detailed research of piecewise desorption in the desorber with a catalyst in the MEA regeneration process is demanded in the future.

The relative heat duty of different catalysts is presented in Figure 3f. As can be seen, MCM-41 and SO₄²⁻/MCM-41 slightly reduced the heat duty by around 10.8 and 17.5% compared with the noncatalytic MEA solution system, respectively. Also, MCM-41-SO₃H-0.2 decreased the heat duty by around 12.4%. In addition, the heat duty of the system with MCM-41-SO₃H-0.4 and MCM-41-SO₃H-0.8 catalysts was reduced by about 28.7 and 29.2%, respectively. It is noteworthy that the MCM-41-SO₃H-0.6 catalyst minimized the heat duty by up to 33.3%, demonstrating its superior MEA regeneration efficiency. In terms of the relative heat duty, the catalytic performance trend was seen to be MCM-41-SO₃H-0.6 > MCM-41-SO₃H-0.8 > MCM-41-SO₃H-0.4 > SO₄²⁻/MCM-41 > MCM-41-SO₃H-0.2 > MCM-41 > no catalyst.

It can be seen that all the catalysts improved the desorption rate and required a lower CO₂ desorption temperature than the conventional CO₂ capture technologies, where the CO₂ desorption temperature is typically more than 100 °C. This factor alone could significantly reduce the energy consumption of MEA solution regeneration. Also, the dimensions of the stripper column, reboiler, and heat exchanger could be minimized. However, it should be observed that the apparatus in this work was simplified and the energy consumption was recorded using the power meter; thus, the measured reduction values of heat duty cannot truly describe the actual stripping column.

To investigate the catalytic performance of MCM-41-SO₃H-0.6 during CO₂ desorption, Raman spectroscopy of CO₂-rich MEA solution with and without the catalyst was performed in the 900–1200 cm⁻¹ region and is presented in Figure 4. The band centers at 1018, 1068, and 1158 cm⁻¹ were used to monitor the relative concentrations of HCO₃⁻, CO₃²⁻, and MEACOO⁻, according to the C–OH stretching, symmetric C–O stretching, and C–N stretching, respectively.⁵¹ As can be seen, in the noncatalytic CO₂-rich MEA solution system, the peak intensity of HCO₃⁻ started to decrease from 1200 s, while that of CO₃²⁻ and MEACOO⁻ decreased gradually with the CO₂ desorption continuing at a very slow rate. However, when the MCM-41-SO₃H-0.6 catalyst was introduced into the CO₂-rich MEA solution, the peak intensities of HCO₃⁻, CO₃²⁻, and MEACOO⁻ decreased at a much higher rate with CO₂ desorption time. Therefore, it can be concluded that the MCM-41-SO₃H-0.6 catalyst can accelerate the proton transfer,

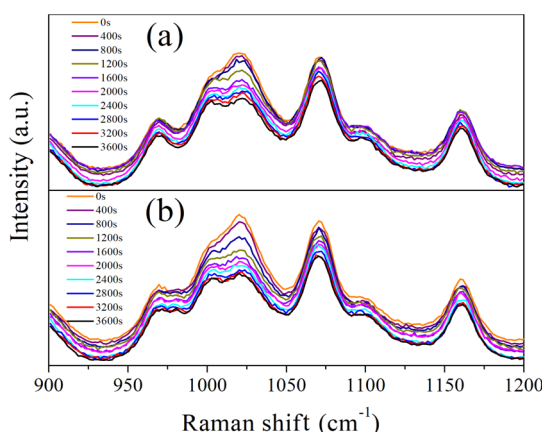
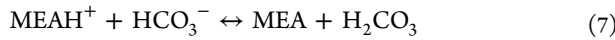
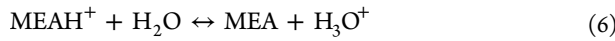
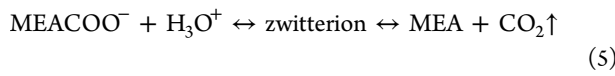


Figure 4. Raman spectra of solutions at different times during CO_2 desorption. (a) MEA without the catalyst. (b) MEA with the MCM-41- SO_3H -0.6 catalyst.

improve the desorption rate, and thus reduce the energy consumption for MEA solution regeneration.

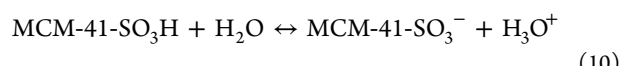
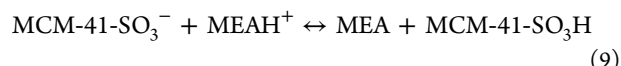
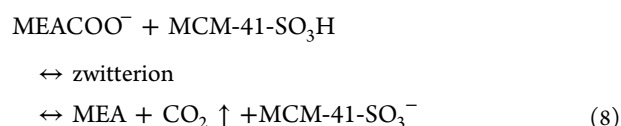
3.3. Catalytic Mechanism and Theoretical Calculations. **3.3.1. Catalytic Mechanism.** The zwitterion mechanism of MEA solution regeneration was proposed by Caplow⁵² and includes two steps, namely, breakdown of carbamate and deprotonation of MEAH^+ as follows:



It is widely believed that the high heat duty of the primary amine is due to two main aspects. On one hand, the deprotonation of MEAH^+ to convert it to MEA essentially does not occur in water because of its activation energy of 73.4 kJ/mol at 25 °C.⁵³ At low temperatures, the shortage of free protons needed for carbamate breakdown means that the reaction hardly takes place. In addition, the reaction of carbamate breakdown is also endothermic with an activation

energy of 15.47 kJ/mol at 25 °C.⁵³ According to the work of Shi *et al.*,²⁴ the existence of the bicarbonate ion (HCO_3^-) could assist the deprotonation of MEAH^+ and reduce the activation energy for proton transfer. Also, Liu *et al.*⁵⁴ reported that the amount of HCO_3^- was limited, and the bicarbonate ion occurred from the CO_2 loading of 0.42 mol CO_2 /mol amine at 20 °C. To sum up, the CO_2 desorption rarely takes place at a low temperatures due to the lack of free protons.

As discussed above, to reduce the heat duty of MEA regeneration, available protons or a medium that could improve proton transfer is necessary to accelerate the CO_2 desorption rate. In this work, when the MCM-41- SO_3H catalysts were added into the CO_2 -rich MEA solution system, the CO_2 desorption rate was enhanced and the energy consumption was reduced. The possible reason is that the sulfonic acid groups on the surface of catalysts act as the Brønsted acid sites and provide free protons. At the same time, the proton-deficient catalysts and AlO_2^- acted as Lewis acid sites, facilitating carrying the proton away from MEAH^+ . The catalytic steps are described as follows:



To describe the details of the catalytic MEA regeneration process, the possible catalytic mechanism over the MCM-41- SO_3H catalyst is proposed and shown in Figure 5. According to the structure of MEACOO^- , one N atom and two O atoms of MEACOO^- were the key positions for CO_2 desorption because it is necessary to break down the C–N bond for CO_2 desorption. Also, the O atoms are an important attachment center for catalysts. Besides, the O atoms can accept the protons from the Brønsted acid sites of the catalysts or the deprotonation of MEAH^+ , which assists the proton transfer. In

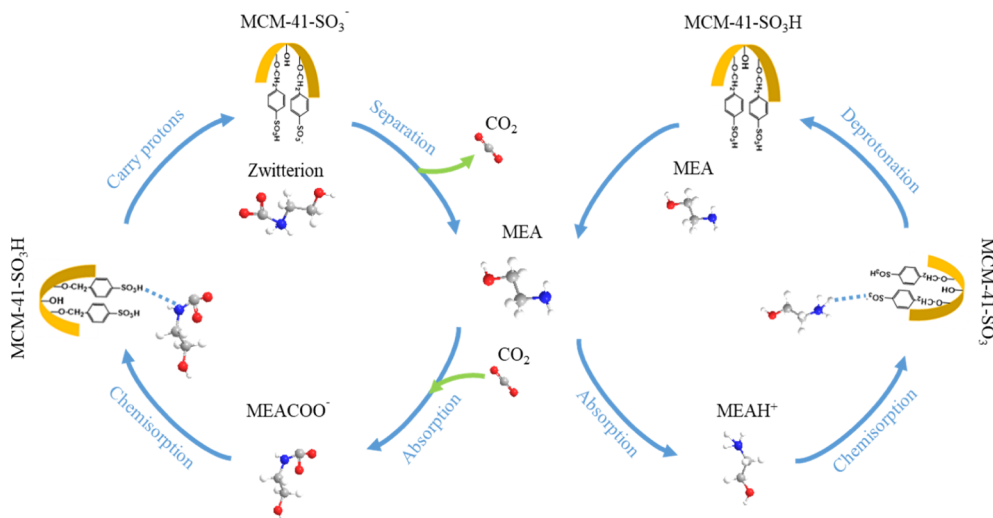


Figure 5. Possible catalytic mechanism for the MCM-41- SO_3H catalyst-assisted carbamate breakdown and promotion of CO_2 released; red, blue, and white balls represent O, N, C, and H, respectively.

detail, the Brønsted acid sites of MCM-41-SO₃H and the deprotonation reaction provide free protons and initially convert MEACOO⁻ to MEACOOH.

Next, the Lewis acid sites on the catalysts such as AlO₂⁻ were chemisorbed onto the O atom, attacking it. Third, the protons on the O atom were transferred to the nearby N atom in an isomerization reaction. After that, the delocalized conjugation of N atoms was destroyed by the protons and converted the configuration of the N atom from sp² to sp³. Consequently, the C–N bond became weak and started to stretch, which does not occur at a relatively low desorption temperature without a catalyst. Last, the C–N bond broke and MEACOOH split into MEA and CO₂. In addition, the proton-deficient catalysts were chemisorbed on MEAH⁺ and took away the protons from MEAH⁺, reducing the activation energy for the deprotonation reaction. After that, MEAH⁺ was changed into MEACOO⁻, and the proton-deficient catalysts were regenerated. In summary, the introduction of MCM-41-SO₃H catalysts into the CO₂-rich MEA solution system provides sufficient free protons and decreases the activation energy for CO₂ desorption, leading to a lower heat duty than in the noncatalytic system.

For the traditional CO₂ desorption, the temperature of amine solution regeneration is typically about 120 °C. High temperatures facilitate the C–N bond breakdown and improve the desorption rate but require a large amount of external heat to increase the system temperature above 100 °C. Additionally, the high heat of vaporization results in further energy costs. In this work, 90 °C was selected as the desorption temperature to reduce the energy consumption for CO₂ capture processes.

3.3.2. Theoretical Calculations. The most stable structures of MCM-41 and MCM-41-SO₃H are shown in Figure 6a–c. Also, the form of acid sites in MCM-41 and MCM-SO₃H are displayed in Figure 6b,c, which shows that the acid sites were mainly correlated with OH groups in MCM-41 and sulfonic acid groups in MCM-41-SO₃H.

As mentioned before, there is the possibility that the sulfonic acid groups of the MCM-41-SO₃H catalyst may donate protons to carbamate and accept protons from MEAH⁺ deprotonation, which may lead to the acceleration of proton-transfer reaction. To prove the catalytic mechanism, density functional theory calculations were employed to assess the reaction enthalpies (ΔH) of CO₂ desorption (MEACOO⁻ + acid sites \leftrightarrow MEA + CO₂ \uparrow) for the two catalysts. Figure 7 shows the calculation model of carbamate decomposition for MCM-41 and MCM-41-SO₃H catalysts. The ΔH is employed as an important evaluation indicator for the activity of CO₂ desorption. As shown in Figure 7, the ΔH of the MCM-41 catalyst calculated was higher than that of the MCM-41-SO₃H catalyst (1.15 vs -0.39 eV), which means that MCM-41-SO₃H is easier to decompose carbamate. Moreover, the BADER electron charges of the acid site H were also calculated before and after MEA regeneration. As shown in Figure 7, the acid site H in MCM-41 and MCM-41-SO₃H donates 0.17 and 0.21 protons, respectively. Therefore, MCM-41-SO₃H shows a better MEA regeneration activity than MCM-41. To sum up, the theoretical calculation results were consistent with the trend of experimental results and proved the possible catalytic mechanism for MEA regeneration with MCM-41-SO₃H by proton-transfer acceleration.

3.4. Structure–Activity Relationship. In addition to the catalytic mechanism above, catalysts' physicochemical properties, including mesopore surface area (MSA) and TAS, may

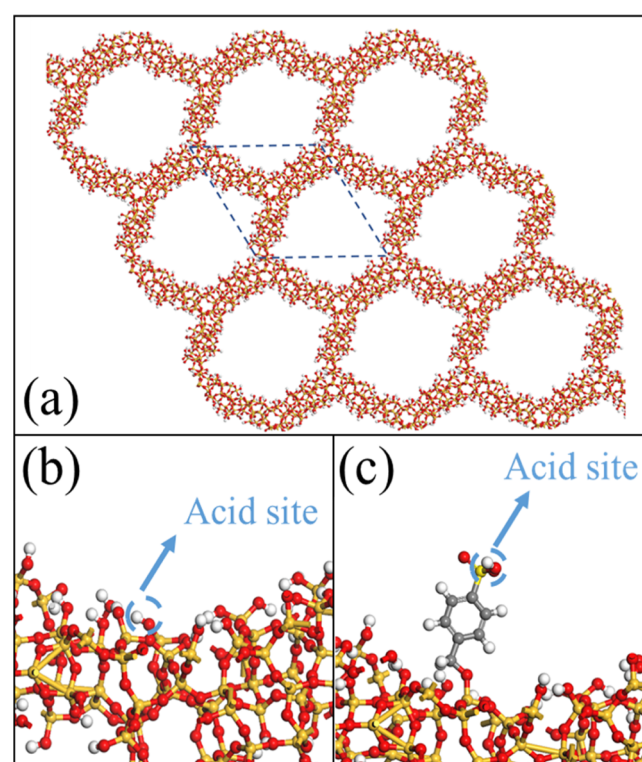


Figure 6. (a) Illustration of the MCM-41 zeolite models (the dash-line-encircled area indicates a unit cell), (b) illustration of the acid site in MCM-41, and (c) illustration of the acid site in MCM-41-SO₃H; red, orange, yellow, gray, and white balls represent O, Si, S, C, and H, respectively.

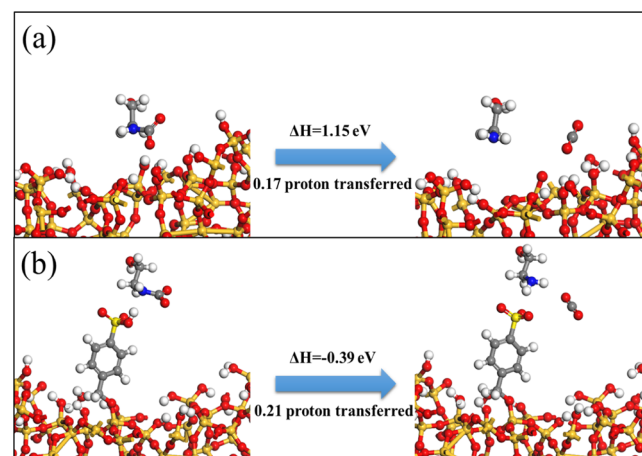


Figure 7. Structures of carbamate decomposition for (a) MCM-41 and (b) MCM-41-SO₃H.

affect the CO₂ desorption reaction. The relationship between the physicochemical properties and heat duty is shown in Figure 8 to investigate the catalytic performance further.

It is well known that a large surface area can have a positive influence on catalytic performance because it can provide a sufficient contact area for the active sites and the reactant. However, it can be seen that the MCM-41-SO₃H-0.2 catalyst possessed the largest mesopore surface and the lowest TAS and it exhibited the worst catalytic performance, indicating that the number of TASs is a critical factor in CO₂ desorption. In addition, the relative heat duty gradually decreased when the

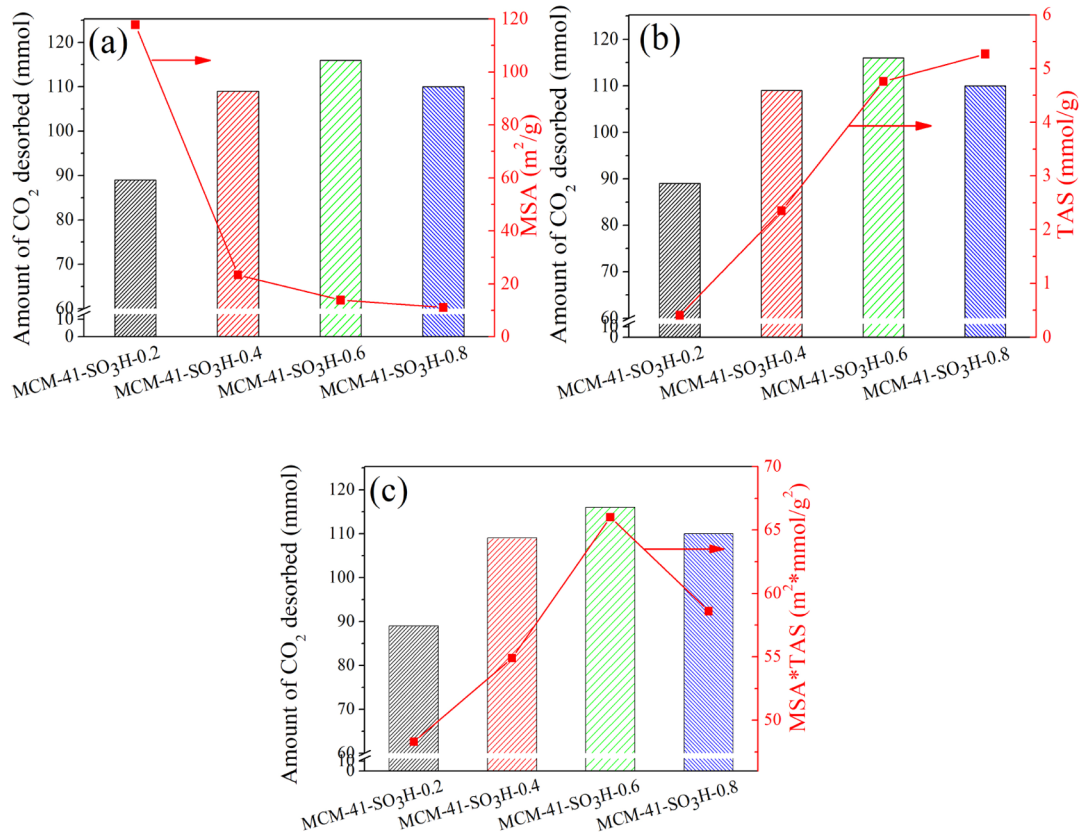


Figure 8. Effect of single and combined catalyst physicochemical properties on CO₂ desorption. (a) Influence of MSA. (b) Influence of TAS. (c) Influence of MSA × TAS.

TASs increased at first, but with the TASs more than 4.76 mmol/g, the relative heat duty increased. The possible reason for this is the decrease of MSA. It is noted that no linear dependence relationship was shown between the MSA and TAS with the relative heat duty. Thus, the relative heat duty may be influenced by the combination properties of MSA × TAS. As shown in Figure 8c, the catalytic performance exhibited a linear dependence relationship with MSA × TAS. The larger the value of MSA × TAS, the lower the relative heat duty for MEA regeneration. The MCM-41-SO₃H-0.6 catalyst had the largest value of MSA × TAS of 66.02 mmol m²/g² and showed the best catalytic properties. Also, the MCM-41-SO₃H-0.2 catalyst had the lowest value of MSA × TAS of 48.30 mmol m²/g² and showed the worst catalytic performance, which could explain the absence of a linear dependence relationship for any single factor. It can be concluded that catalysts with a large MSA and abundant TASs would have a superior catalytic performance, and the value of MSA × TAS plays a significant role in evaluating the catalytic activity. Further work is required to quantify the type of acid sites for the MEA regeneration over the functionalized catalysts in the future.

3.5. Catalyst Stability Test. The stability of the MCM-41-SO₃H-0.6 catalyst was evaluated by recycling the catalyst from the MEA solution and reusing it for five runs. The experimental conditions were consistent with the CO₂ desorption test aforementioned. After each CO₂ desorption experiment run, the catalysts were separated from MEA solution by centrifugation, washed with deionized water, and then dried in an oven to remove the amine vapor residual on the surface of the catalysts. The recovered catalyst was reused

for the next CO₂ desorption test with fresh CO₂-rich MEA solution under the same conditions, and a small amount of the fresh catalyst was added to make up for the loss of the catalyst during the recycle processes. The reusability performance of the MCM-41-SO₃H-0.6 catalyst is shown in Figure 9. As can

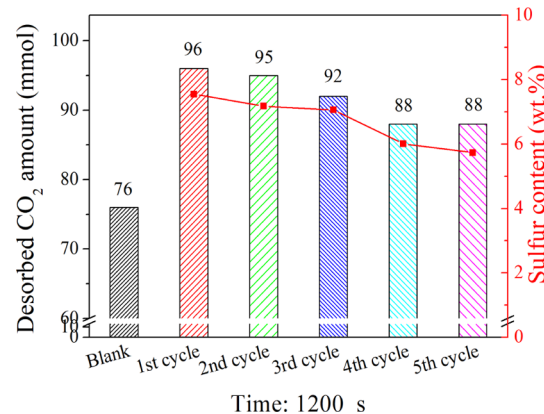


Figure 9. Stability during the cyclic tests of the MCM-41-SO₃H-0.6 catalyst.

be seen, after five cycles, the amount of CO₂ desorbed decreased from 96 to 88 mmol, only a slight decrease. This decrease in catalytic performance may be ascribed to the loss of sulfur across the MCM-41 molecular sieve surface. To further support this conclusion, the sulfur contents of the MCM-41-SO₃H-0.6 catalyst after the cycle experiment were measured. As presented in Figure 9, the sulfur contents decreased from

7.6 to 5.7 wt % as the number of cycles increased, which is consistent with the slightly decreasing trend of the amount of CO₂ released. Also, the sulfur content of the fresh MCM-41-SO₃H-0.6 catalyst can be as high as 8.8 wt %, which is higher than that of the recovered catalyst in comparison. This fact indicated that the loss of sulfur over the catalyst surface might be an important reason for MCM-41-SO₃H-0.6 catalyst deactivation. Therefore, reducing sulfur leaching in the cycle experiment to further increase the stability of the catalyst is the direction of future work. Overall, the MCM-41-SO₃H-0.6 catalyst is stable and regenerates easily, showing potential for use in industrial applications for CO₂ capture.

4. CONCLUSIONS

In summary, this study investigated the catalytic performance of the MCM-41-SO₃H catalysts with varied acid sites, including the CO₂ desorption rate, CO₂ desorbed amount, and relative heat duty. A feasible catalytic mechanism for the MCM-41-SO₃H catalysts was proposed to analyze the catalytic MEA solution regeneration process. Moreover, the effect of different physicochemical properties and the stability of catalysts were also systematically studied.

- (1) The MCM-41-SO₃H-0.6 catalyst exhibited the best catalytic activity in CO₂ desorption, reducing the relative heat duty by 33.3% and enhancing the instantaneous desorption rate by up to 195%.
- (2) The combination of the properties of MSA × TAS is an important factor to enhance the CO₂ desorption rate.
- (3) The MCM-41-SO₃H-0.6 catalyst possesses excellent stability and can be easily regenerated for reuse in CO₂ desorption.

■ ASSOCIATED CONTENT

Supporting Information

The Supporting Information is available free of charge at <https://pubs.acs.org/doi/10.1021/acs.iecr.1c03671>.

Textural properties of studied solid acid catalysts, cyclic capacity for the catalyst-MEA systems at different regeneration times, brief review of MEA catalytic regeneration, mass balance for CO₂ desorption tests, and influence of MSA × TAS on heat duty ([PDF](#))

■ AUTHOR INFORMATION

Corresponding Authors

Hongxia Gao — Joint International Center for CO₂ Capture and Storage (iCCS), Provincial Hunan Key Laboratory for Cost-Effective Utilization of Fossil Fuel Aimed at Reducing CO₂ Emissions, College of Chemistry and Chemical Engineering, Hunan University, Changsha 410082, PR China; Email: hxgao@hnu.edu.cn

Zhiwu Liang — Joint International Center for CO₂ Capture and Storage (iCCS), Provincial Hunan Key Laboratory for Cost-Effective Utilization of Fossil Fuel Aimed at Reducing CO₂ Emissions, College of Chemistry and Chemical Engineering, Hunan University, Changsha 410082, PR China; [ORCID: 0000-0003-1935-0759](https://orcid.org/0000-0003-1935-0759); Email: zwliang@hnu.edu.cn

Authors

Qiang Sun — Joint International Center for CO₂ Capture and Storage (iCCS), Provincial Hunan Key Laboratory for Cost-Effective Utilization of Fossil Fuel Aimed at Reducing CO₂

Emissions, College of Chemistry and Chemical Engineering, Hunan University, Changsha 410082, PR China

Tianhao Li — Joint International Center for CO₂ Capture and Storage (iCCS), Provincial Hunan Key Laboratory for Cost-Effective Utilization of Fossil Fuel Aimed at Reducing CO₂ Emissions, College of Chemistry and Chemical Engineering, Hunan University, Changsha 410082, PR China

Yu Mao — Joint International Center for CO₂ Capture and Storage (iCCS), Provincial Hunan Key Laboratory for Cost-Effective Utilization of Fossil Fuel Aimed at Reducing CO₂ Emissions, College of Chemistry and Chemical Engineering, Hunan University, Changsha 410082, PR China

Teerawat Sema — Department of Chemical Technology, Faculty of Science, Chulalongkorn University, Bangkok 10330, Thailand; [ORCID: 0000-0002-1390-3992](https://orcid.org/0000-0002-1390-3992)

Shengyu Wang — Joint International Center for CO₂ Capture and Storage (iCCS), Provincial Hunan Key Laboratory for Cost-Effective Utilization of Fossil Fuel Aimed at Reducing CO₂ Emissions, College of Chemistry and Chemical Engineering, Hunan University, Changsha 410082, PR China

Libin Liu — Joint International Center for CO₂ Capture and Storage (iCCS), Provincial Hunan Key Laboratory for Cost-Effective Utilization of Fossil Fuel Aimed at Reducing CO₂ Emissions, College of Chemistry and Chemical Engineering, Hunan University, Changsha 410082, PR China

Complete contact information is available at:

<https://pubs.acs.org/10.1021/acs.iecr.1c03671>

Notes

The authors declare no competing financial interest.

■ ACKNOWLEDGMENTS

The financial support from the National Natural Science Foundation of China (NSFC-Nos. 22138002, 22078083, 21978075, and 21878073), the Hunan Key R & D Program Project (2020NK2015), the National Key R&D Projects in Changsha (kh2005018), the Science and Technology Innovation Program of Hunan Province (2020RC5032), the China Outstanding Engineer Training Plan for Students of Chemical Engineering and Technology in Hunan University (MOE-No. 2011-40), and the Hunan Provincial Innovation Foundation for Postgraduate (CX20200447) is acknowledged.

■ REFERENCES

- (1) Szulejko, J. E.; Kumar, P.; Deep, A.; Kim, K.-H. Global warming projections to 2100 using simple CO₂ greenhouse gas modeling and comments on CO₂ climate sensitivity factor. *Atmos. Pollut. Res.* **2017**, *8*, 136–140.
- (2) Bui, M.; Adjiman, C. S.; Bardow, A.; Anthony, E. J.; Boston, A.; Brown, S.; Fennell, P. S.; Fuss, S.; Galindo, A.; Hackett, L. A.; Hallett, J. P.; Herzog, H. J.; Jackson, G.; Kemper, J.; Krevor, S.; Maitland, G. C.; Matuszewski, M.; Metcalfe, I. S.; Petit, C.; Puxty, G.; Reimer, J.; Reiner, D. M.; Rubin, E. S.; Scott, S. A.; Shah, N.; Smit, B.; Trusler, J. P. M.; Webley, P.; Wilcox, J.; Mac Dowell, N. Carbon capture and storage (CCS): the way forward. *Energy Environ. Sci.* **2018**, *11*, 1062–1176.
- (3) Rogelj, J.; den Elzen, M.; Höhne, N.; Fransen, T.; Fekete, H.; Winkler, H.; Schaeffer, R.; Sha, F.; Riahi, K.; Meinshausen, M. Paris Agreement climate proposals need a boost to keep warming well below 2 degrees C. *Nature* **2016**, *534*, 631–639.
- (4) MacDowell, N.; Florin, N.; Buchard, A.; Hallett, J.; Galindo, A.; Jackson, G.; Adjiman, C. S.; Williams, C. K.; Shah, N.; Fennell, P. An

- overview of CO₂ capture technologies. *Energy Environ. Sci.* **2010**, *3*, 1645–1669.
- (5) Yu, C.-H.; Huang, C.-H.; Tan, C.-S. A review of CO₂ capture by absorption and adsorption. *Aerosol Air Qual. Res.* **2012**, *12*, 745–769.
- (6) Yang, X.; Rees, R. J.; Conway, W.; Puxty, G.; Yang, Q.; Winkler, D. A. Computational modeling and simulation of CO₂ capture by aqueous amines. *Chem. Rev.* **2017**, *117*, 9524–9593.
- (7) Dutcher, B.; Fan, M.; Russell, A. G. Amine-based CO₂ capture technology development from the beginning of 2013—A Review. *ACS Appl. Mater. Interfaces* **2015**, *7*, 2137–2148.
- (8) Luis, P. Use of monoethanolamine (MEA) for CO₂ capture in a global scenario: Consequences and alternatives. *Desalination* **2016**, *380*, 93–99.
- (9) Freguia, S.; Rochelle, G. T. Modeling of CO₂ capture by aqueous monoethanolamine. *AIChE J.* **2003**, *49*, 1676–1686.
- (10) Zhang, X.; Liu, H.; Liang, Z.; Idem, R.; Tontiwachwuthikul, P.; Jaber Al-Marri, M.; Benamor, A. Reducing energy consumption of CO₂ desorption in CO₂-loaded aqueous amine solution using Al₂O₃/HZSM-5 bifunctional catalysts. *Appl. Energy* **2018**, *229*, 562–576.
- (11) Zhang, X.; Zhang, R.; Liu, H.; Gao, H.; Liang, Z. Evaluating CO₂ desorption performance in CO₂-loaded aqueous tri-solvent blend amines with and without solid acid catalysts. *Appl. Energy* **2018**, *218*, 417–429.
- (12) Bairq, Z. A. S.; Gao, H.; Huang, Y.; Zhang, H.; Liang, Z. Enhancing CO₂ desorption performance in rich MEA solution by addition of SO₄²⁻/ZrO₂/SiO₂ bifunctional catalyst. *Appl. Energy* **2019**, *252*, 113440.
- (13) Oexmann, J.; Kather, A. Minimising the regeneration heat duty of post-combustion CO₂ capture by wet chemical absorption: The misguided focus on low heat of absorption solvents. *Int. J. Greenhouse Gas Control* **2010**, *4*, 36–43.
- (14) Puxty, G.; Rowland, R.; Allport, A.; Yang, Q.; Bown, M.; Burns, R.; Maeder, M.; Attalla, M. Carbon dioxide postcombustion capture: a novel screening study of the carbon dioxide absorption performance of 76 amines. *Environ. Sci. Technol.* **2009**, *43*, 6427–6433.
- (15) Liu, H.; Xiao, M.; Liang, Z.; Tontiwachwuthikul, P. The analysis of solubility, absorption kinetics of CO₂ absorption into aqueous 1-diethylamino-2-propanol solution. *AIChE J.* **2017**, *63*, 2694–2704.
- (16) Li, Q.; Gao, H.; Liu, S.; Lv, J.; Liang, Z. Novel thermodynamic model for vapor-liquid equilibrium of CO₂ in aqueous solution of 4-(ethyl-methyl-amino)-2-butanol with designed structures. *Chem. Eng. Sci.* **2020**, *218*, 115557.
- (17) Zhang, R.; Zhang, X.; Yang, Q.; Yu, H.; Liang, Z.; Luo, X. Analysis of the reduction of energy cost by using MEA-MDEA-PZ solvent for post-combustion carbon dioxide capture (PCC). *Appl. Energy* **2017**, *205*, 1002–1011.
- (18) Saric, S.; Biggs, B.; Janbahan, M.; Hamilton, R.; Do, H. K.; Mayoral, S.; Haan, J. L. An integrated device to convert carbon dioxide to energy. *Appl. Energy* **2016**, *183*, 1346–1350.
- (19) Gao, H.; Zhou, L.; Liang, Z.; Idem, R. O.; Fu, K.; Sema, T.; Tontiwachwuthikul, P. Comparative studies of heat duty and total equivalent work of a new heat pump distillation with split flow process, conventional split flow process, and conventional baseline process for CO₂ capture using monoethanolamine. *Int. J. Greenhouse Gas Control* **2014**, *24*, 87–97.
- (20) Liang, Z.; Gao, H.; Rongwong, W.; Na, Y. Comparative studies of stripper overhead vapor integration-based configurations for post-combustion CO₂ capture. *Int. J. Greenhouse Gas Control* **2015**, *34*, 75–84.
- (21) Zhou, X.; Shen, Y.; Liu, F.; Ye, J.; Wang, X.; Zhao, J.; Zhang, S.; Wang, L.; Li, S.; Chen, J. A Novel Dual-Stage Phase Separation Process for CO₂ Absorption into a Biphasic Solvent with Low Energy Penalty. *Environ. Sci. Technol.* **2021**, *55*, 15313–15322.
- (22) Jiang, C.; Chen, H.; Wang, J.; Shen, Y.; Ye, J.; Zhang, S.; Wang, L.; Chen, J. Phase Splitting Agent Regulated Biphasic Solvent for Efficient CO₂ Capture with a Low Heat Duty. *Environ. Sci. Technol.* **2020**, *54*, 7601–7610.
- (23) Ye, J.; Jiang, C.; Chen, H.; Shen, Y.; Zhang, S.; Wang, L.; Chen, J. Novel Biphasic Solvent with Tunable Phase Separation for CO₂ Capture: Role of Water Content in Mechanism, Kinetics, and Energy Penalty. *Environ. Sci. Technol.* **2019**, *53*, 4470–4479.
- (24) Shi, H.; Naami, A.; Idem, R.; Tontiwachwuthikul, P. Catalytic and non catalytic solvent regeneration during absorption-based CO₂ capture with single and blended reactive amine solvents. *Int. J. Greenhouse Gas Control* **2014**, *26*, 39–50.
- (25) Xing, L.; Wei, K.; Li, Q.; Wang, R.; Zhang, S.; Wang, L. One-Step Synthesized SO₄²⁻/ZrO₂-HZSM-5 Solid Acid Catalyst for Carbamate Decomposition in CO₂ Capture. *Environ. Sci. Technol.* **2020**, *54*, 13944–13952.
- (26) Zhang, X.; Huang, Y.; Yang, J.; Gao, H.; Huang, Y.; Luo, X.; Liang, Z.; Tontiwachwuthikul, P. Amine-based CO₂ capture aided by acid-basic bifunctional catalyst: Advancement of amine regeneration using metal modified MCM-41. *Chem. Eng. J.* **2020**, *383*, 123077.
- (27) Idem, R.; Shi, H.; Gelowitz, D.; Tontiwachwuthikul, P. Catalytic method and apparatus for separating a gaseous component from an incoming gas stream. U.S. Patent 20,130,108,532 A1, 2011.
- (28) Feng, B.; Du, M.; Dennis, T. J.; Anthony, K.; Perumal, M. J. Reduction of energy requirement of CO₂ desorption by adding acid into CO₂-loaded solvent. *Energy Fuels* **2010**, *24*, 213–219.
- (29) Li, K.; van der Poel, P.; Conway, W.; Jiang, K.; Puxty, G.; Yu, H.; Feron, P. Mechanism investigation of advanced metal–ion-mediated amine regeneration: a novel pathway to reducing CO₂ reaction enthalpy in amine-based CO₂ capture. *Environ. Sci. Technol.* **2018**, *S2*, 14538–14546.
- (30) Alivand, M. S.; Mazaheri, O.; Wu, Y.; Stevens, G. W.; Scholes, C. A.; Mumford, K. A. Catalytic Solvent Regeneration for Energy-Efficient CO₂ Capture. *ACS Sustainable Chem. Eng.* **2020**, *8*, 18755–18788.
- (31) Xing, L.; Wei, K.; Li, Y.; Fang, Z.; Li, Q.; Qi, T.; An, S.; Zhang, S.; Wang, L. TiO₂ Coating Strategy for Robust Catalysis of the Metal–Organic Framework toward Energy-Efficient CO₂ Capture. *Environ. Sci. Technol.* **2021**, *55*, 11216–11224.
- (32) Sahoo, P. C.; Kumar, M.; Singh, A.; Singh, M. P.; Puri, S. K. Biocatalyzed accelerated post-combustion CO₂ capture and stripping in monoethanolamine. *Energy Fuels* **2017**, *31*, 11007–11012.
- (33) Bhatti, U. H.; Shah, A. K.; Kim, J. N.; You, J. K.; Choi, S. H.; Lim, D. H.; Nam, S.; Park, Y. H.; Baek, I. H. Effects of transition metal oxide catalysts on MEA solvent regeneration for the post-combustion carbon capture process. *ACS Sustainable Chem. Eng.* **2017**, *5*, 5862–5868.
- (34) Bhatti, U. H.; Nam, S.; Park, S.; Baek, I. H. Performance and mechanism of metal oxide catalyst-aided amine solvent regeneration. *ACS Sustainable Chem. Eng.* **2018**, *6*, 12079–12087.
- (35) Zhang, X.; Zhang, X.; Liu, H.; Li, W.; Xiao, M.; Gao, H.; Liang, Z. Reduction of energy requirement of CO₂ desorption from a rich CO₂-loaded MEA solution by using solid acid catalysts. *Appl. Energy* **2017**, *202*, 673–684.
- (36) Lai, Q.; Toan, S.; Assiri, M. A.; Cheng, H.; Russell, A. G.; Adidharma, H.; Radosz, M.; Fan, M. Catalyst-TiO₂(OH)₂ could drastically reduce the energy consumption of CO₂ capture. *Nat. Commun.* **2018**, *9*, 2672.
- (37) Davis, M. E. Ordered porous materials for emerging applications. *Nature* **2002**, *417*, 813–821.
- (38) Zhang, X.; Huang, Y.; Gao, H.; Luo, X.; Liang, Z.; Tontiwachwuthikul, P. Zeolite catalyst-aided tri-solvent blend amine regeneration: An alternative pathway to reduce the energy consumption in amine-based CO₂ capture process. *Appl. Energy* **2019**, *240*, 827–841.
- (39) Bhatti, U. H.; Shah, A. K.; Hussain, A.; Khan, H. A.; Park, C. Y.; Nam, S. C.; Baek, I. H. Catalytic activity of facilely synthesized mesoporous HZSM-5 catalysts for optimizing the CO₂ desorption rate from CO₂-rich amine solutions. *Chem. Eng. J.* **2020**, *389*, 123439.
- (40) Gao, H.; Huang, Y.; Zhang, X.; Bairq, Z. A. S.; Huang, Y.; Tontiwachwuthikul, P.; Liang, Z. Catalytic performance and mechanism of SO₄²⁻/ZrO₂/SBA-15 catalyst for CO₂ desorption in

CO₂-loaded monoethanolamine solution. *Appl. Energy* **2020**, *259*, 114179.

(41) Sheng, X.; Gao, J.; Han, L.; Jia, Y.; Sheng, W. One-pot synthesis of tryptophols with mesoporous MCM-41 silica catalyst functionalized with sulfonic acid groups. *Microporous Mesoporous Mater.* **2011**, *143*, 73–77.

(42) Perdew, J. P.; Burke, K.; Ernzerhof, M. Generalized Gradient Approximation Made Simple. *Phys. Rev. Lett.* **1996**, *77*, 3865–3868.

(43) Kresse, G.; Furthmüller, J. Efficiency of ab-initio total energy calculations for metals and semiconductors using a plane-wave basis set. *Comput. Mater. Sci.* **1996**, *6*, 15–50.

(44) Kresse, G.; Hafner, J. Ab initio molecular-dynamics simulation of the liquid-metal–amorphous-semiconductor transition in germanium. *Phys. Rev. B: Condens. Matter Mater. Phys.* **1994**, *49*, 14251–14269.

(45) Klimeš, J.; Bowler, D. R.; Michaelides, A. J. P. R. B. Van der Waals density functionals applied to solids. *Phys. Rev. B: Condens. Matter Mater. Phys.* **2011**, *83*, 195131.

(46) Kresse, G.; Joubert, D. From ultrasoft pseudopotentials to the projector augmented-wave method. *Phys. Rev. B: Condens. Matter Mater. Phys.* **1999**, *59*, 1758–1775.

(47) Blöchl, P. E.; Jepsen, O.; Andersen, O. K. Improved Tetrahedron Method for Brillouin-Zone Integrations. *Phys. Rev. B: Condens. Matter Mater. Phys.* **1994**, *49*, 16223.

(48) Horwitz, W. J. *Association of Official Analytical Chemists (AOAC) Methods*; George Banta Company: Menasha, WI, 1975.

(49) Lima, E. T. L.; Queiroz, L. S.; Pires, L. H. D.; Angelica, R. S.; da Costa, C. E. F.; Zamian, J. R.; da Rocha Filho, G. N.; Luque, R.; do Nascimento, L. A. S. Valorization of Mining Waste in the Synthesis of Organofunctionalized Aluminosilicates for the Esterification of Waste from Palm Oil Deodorization. *ACS Sustainable Chem. Eng.* **2019**, *7*, 7543–7551.

(50) Zhang, J. J.; Wang, W. Y.; Wang, G. J.; Song, H.; Wang, L. Preparation of Solid Superacid Catalysts and Oil Oxidative Desulfurization Using K₂FeO₄. *Russ. J. Appl. Chem.* **2018**, *91*, 1513–1519.

(51) Wong, M. K.; Bustam, M. A.; Shariff, A. M. Chemical speciation of CO₂ absorption in aqueous monoethanolamine investigated by in situ Raman spectroscopy. *Int. J. Greenhouse Gas Control* **2015**, *39*, 139–147.

(52) Caplow, M. Kinetics of carbamate formation and breakdown. *J. Am. Chem. Soc.* **1968**, *90*, 6795–6803.

(53) Zhang, X.; Hong, J.; Liu, H.; Luo, X.; Olson, W.; Tontiwachwuthikul, P.; Liang, Z. SO₄²⁻/ZrO₂ supported on γ-Al₂O₃ as a catalyst for CO₂ desorption from CO₂-loaded monoethanolamine solutions. *AIChE J.* **2018**, *64*, 3988–4001.

(54) Liu, H.; Zhang, X.; Gao, H.; Liang, Z.; Idem, R.; Tontiwachwuthikul, P. Investigation of CO₂ regeneration in single and blended amine solvents with and without catalyst. *Ind. Eng. Chem. Res.* **2017**, *S6*, 7656–7664.